

Supporting Information

Influence of ligand architecture in tuning reaction bifurcation pathways for chlorite oxidation by nonheme iron complexes.

Prasenjit Barman,[†] Abayomi S. Faponle,[‡] Anil Kumar Vardhaman,[†] Davide Angelone,[⊥] Anna-Maria Löhr,[◊] Wesley R. Browne,[⊥] Peter Comba,^{*◊} Chivukula V. Sastri^{*†} and Sam P. de Visser^{*‡}

[†] Department of Chemistry, Indian Institute of Technology Guwahati, 781039, Assam, India

[⊥] Stratingh Institute for Chemistry, Faculty of Mathematics and Natural Sciences, University of Groningen, Nijenborgh 4, 9747 AG Groningen, The Netherlands

[◊] Heidelberg University, Anorganisch-Chemisches Institut and Interdisciplinary Center for Scientific Computing (IWR), Im Neuenheimer Feld 270, 69120 Heidelberg, Germany

^{*} Manchester Institute of Biotechnology and School of Chemical Engineering and Analytical Science, The University of Manchester, 131 Princess Street, Manchester M1 7DN, United Kingdom

Corresponding Author

* Sam de Visser (sam.devisser@manchester.ac.uk);
Chivukula V. Sastri (sastricv@iitg.ernet.in);
Peter Comba (peter.comba@aci.uni-heidelberg.de)

Full reference for Gaussian-09: *Gaussian* 09, Revision D.01, Frisch, M. J.; Trucks, G. W.; Schlegel, H. B.; Scuseria, G. E.; Robb, M. A.; Cheeseman, J. R.; Scalmani, G.; Barone, V.; Mennucci, B.; Petersson, G. A.; Nakatsuji, H.; Caricato, M.; Li, X.; Hratchian, H. P.; Izmaylov, A. F.; Bloino, J.; Zheng, G.; Sonnenberg, J. L.; Hada, M.; Ehara, M.; Toyota, K.; Fukuda, R.; Hasegawa, J.; Ishida, M.; Nakajima, T.; Honda, Y.; Kitao, O.; Nakai, H.; Vreven, T.; Montgomery Jr, J. A.; Peralta, J. E.; Ogliaro, F.; Bearpark, M.; Heyd, J. J.; Brothers, E.; Kudin, K. N.; Staroverov, V. N.; Keith, T.; Kobayashi, R.; Normand, J.; Raghavachari, K.; Rendell, A.; Burant, J. C.; Iyengar, S. S.; Tomasi, J.; Cossi, M.; Rega, N.; Millam, J. M.; Klene, M.; Knox, J. E.; Cross, J. B.; Bakken, V.; Adamo, C.; Jaramillo, J.; Gomperts, R.; Stratmann, R. E.; Yazyev, O.; Austin, A. J.; Cammi, R.; Pomelli, C.; Ochterski, J. W.; Martin, R. L.; Morokuma, K.; Zakrzewski, V. G.; Voth, G. A.; Salvador, P.; Dannenberg, J. J.; Dapprich, S.; Daniels, A. D.; Farkas, O.; Foresman, J. B.; Ortiz, J. V.; Cioslowski, J.; Fox, D. J. *Gaussian*, Inc., Wallingford CT, 2013..

Part I: Experimental Data with Reaction Kinetics and Spectroscopic Characterization of Products and Intermediates.

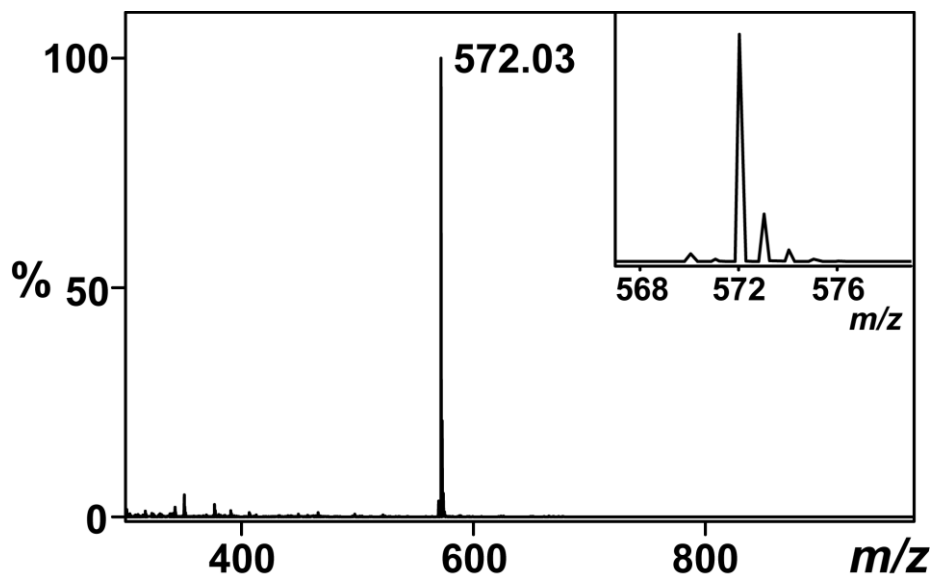


Figure S1. Electrospray ionization mass spectra of $[\text{Fe}^{\text{II}}(\text{CH}_3\text{CN})(\text{N}4\text{Py})](\text{CF}_3\text{SO}_3)_2$. The peak assigned for $m/z = 572.03$ corresponds to $[\text{Fe}^{\text{II}}(\text{CF}_3\text{SO}_3)(\text{N}4\text{Py})]^+$ in CH_3CN at 298 K.

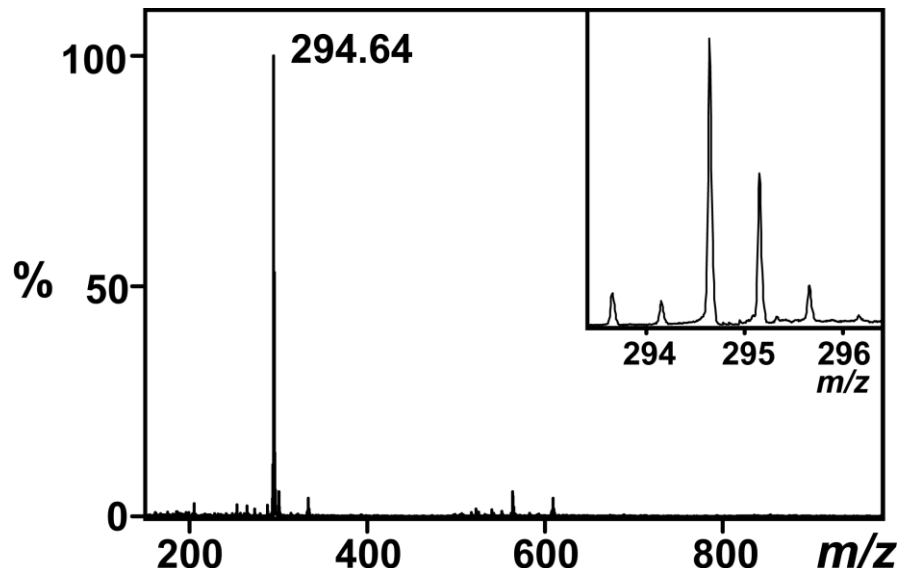


Figure S2. Electrospray ionization mass spectra of $[\text{Fe}^{\text{II}}(\text{CH}_3\text{CN})(\text{L}^1)](\text{BF}_4)_2$. The peak assigned for $m/z = 294.64$ corresponds to $[\text{Fe}^{\text{II}}(\text{L}^1)]^{2+}$ in CH_3CN at 298 K.

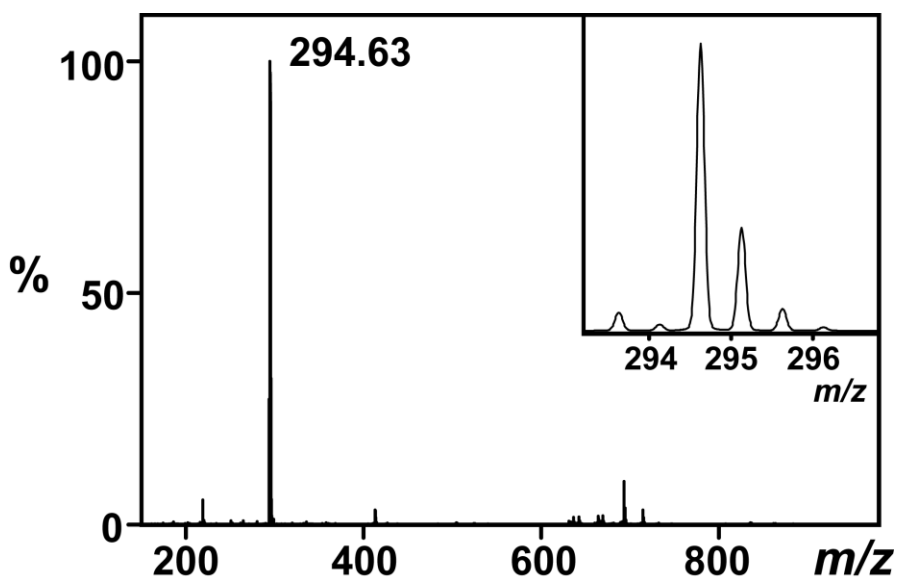


Figure S3. Electrospray ionization mass spectra of $[\text{Fe}^{\text{II}}(\text{CH}_3\text{CN})(\text{L}^2)](\text{BF}_4)_2$. The peaks assigned for $m/z = 294.63$ correspond to $[\text{Fe}^{\text{II}}(\text{L}^2)]^{2+}$ in CH_3CN at 298 K.

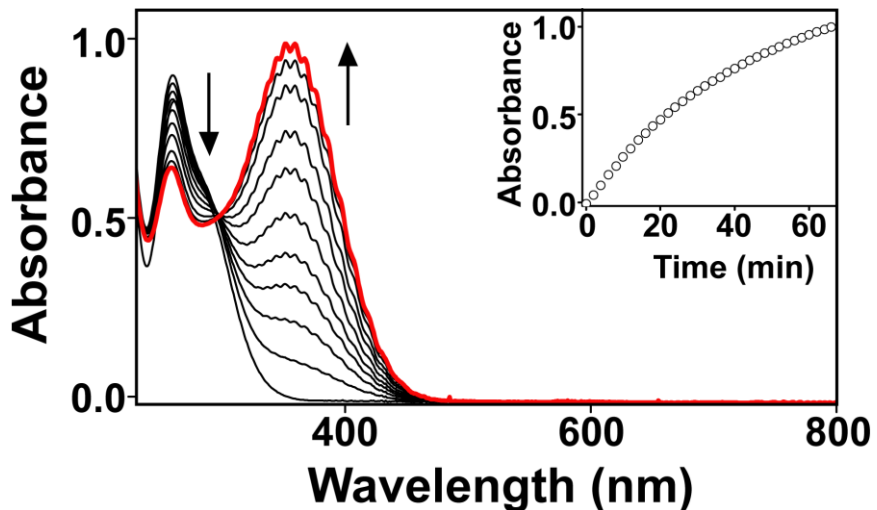


Figure S4. UV-vis spectral changes for the reaction of $10 \mu\text{M} [\text{Fe}^{\text{II}}(\text{L}^2)]^{2+}$ with 8.0 mM NaClO_2 . Inset shows the time trace for the formation of ClO_2 at 298 K and $\text{pH} = 5.0$ in acetate buffer. Scan interval was 120 s .

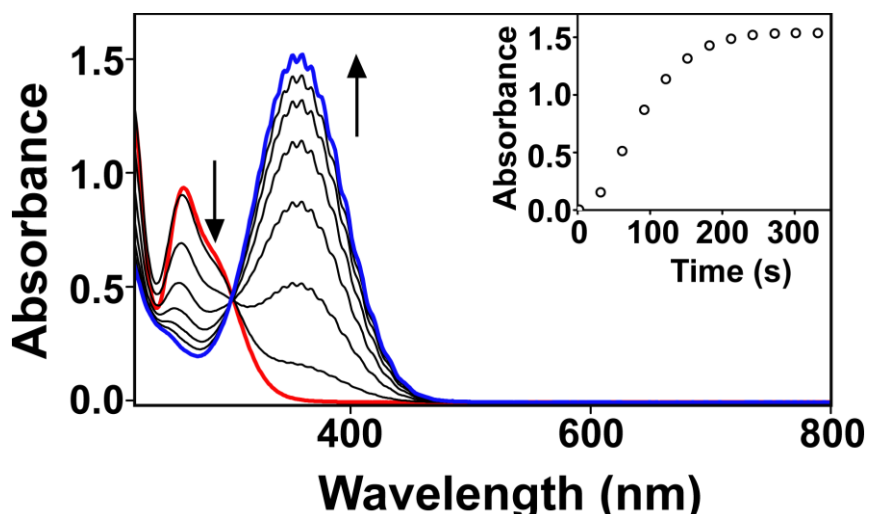


Figure S5. UV-vis spectral changes for the reaction of $10 \mu\text{M} [\text{Fe}^{\text{II}}(\text{N4Py})]^{2+}$ with 8.0 mM NaClO_2 . Inset shows the time trace for the formation of ClO_2 at 298 K and $\text{pH} = 5.0$ in acetate buffer. Scan interval was 30 s .

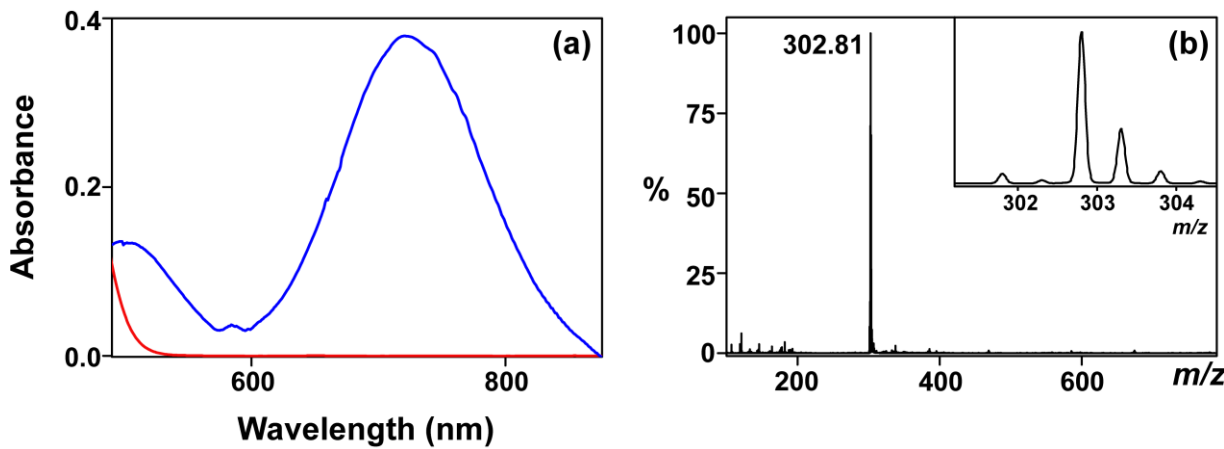


Figure S6. (a) UV-vis spectra of the iron(IV)-oxo formation for the reaction of 1 mM $[\text{Fe}^{\text{II}}(\text{L}^2)]^{2+}$ with 1.2 equiv. of NaClO_2 at 298 K and $\text{pH} = 5.0$ in acetate buffer. (b) ESI-MS spectra of $[\text{Fe}^{\text{IV}}(\text{O})(\text{L}^2)]^{2+}$.

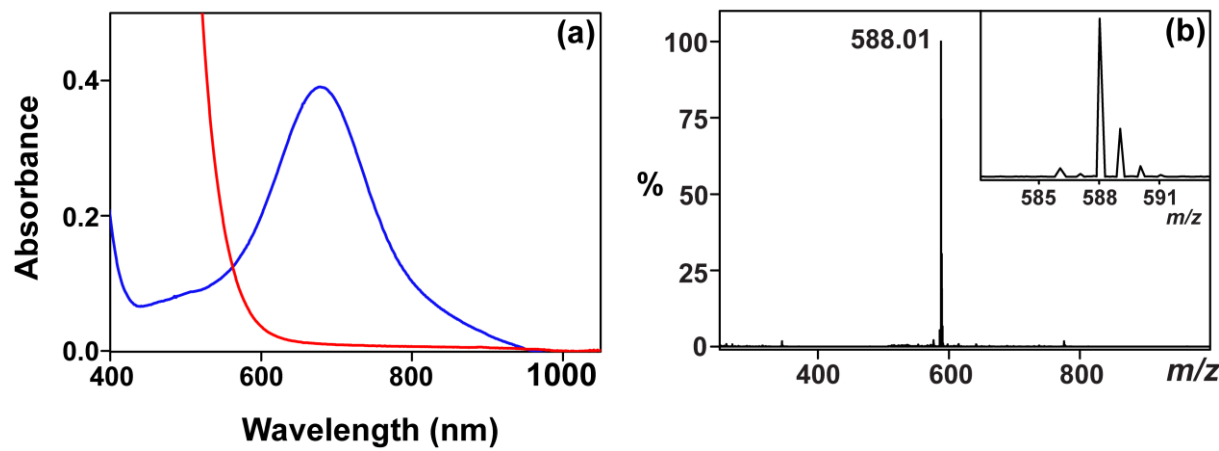


Figure S7. (a) UV-vis spectra of the iron(IV)-oxo formation for the reaction of 1 mM $[\text{Fe}^{\text{II}}(\text{N4Py})]^{2+}$ with 1.2 equiv. of NaClO_2 at 298 K and $\text{pH} = 5.0$ in acetate buffer. (b) ESI-MS spectra of $[\text{Fe}^{\text{IV}}(\text{O})(\text{N4Py})]^{2+}$.

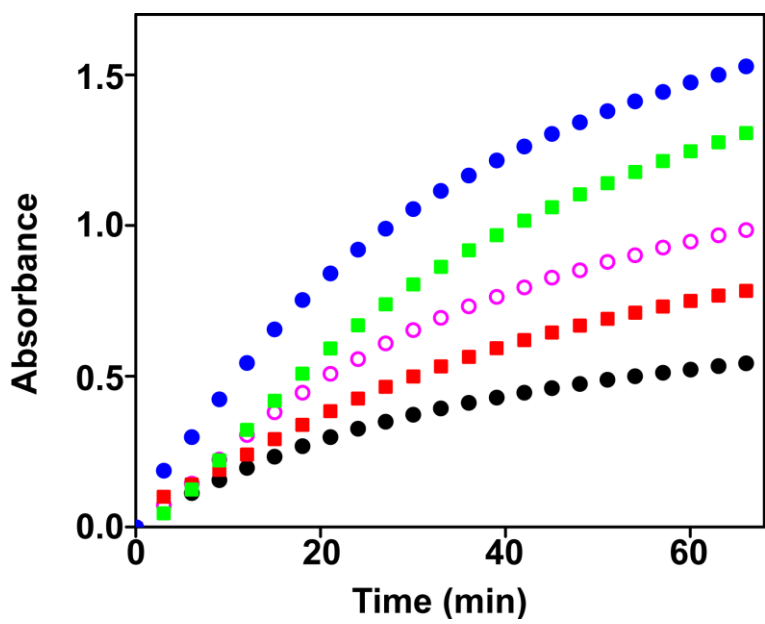


Figure S8. Formation of ClO_2 versus time. Experimental conditions: $[\text{Fe}^{\text{II}}(\text{L}^1)]^{2+} = 50 \mu\text{M}$; $[\text{ClO}_2^-] = 10.0, 8.0, 6.0, 4.0$, and 2.0 mM (top to bottom).

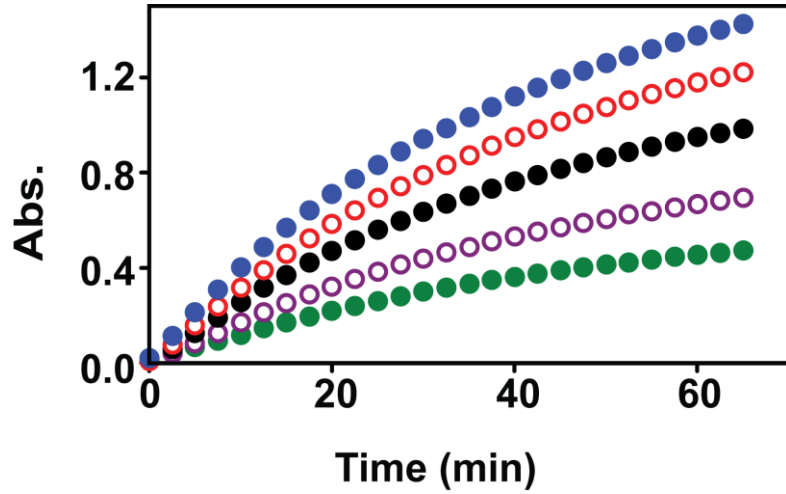


Figure S9. Absorbance changes at 360 nm as a function of time. Reaction conditions: $[\text{Fe}^{\text{II}}(\text{L}^2)]^{2+} = 10 \mu\text{M}$; $[\text{ClO}_2^-] = 12.0, 10.0, 8.0, 6.0, 4.0 \text{ mM}$ (top to bottom).

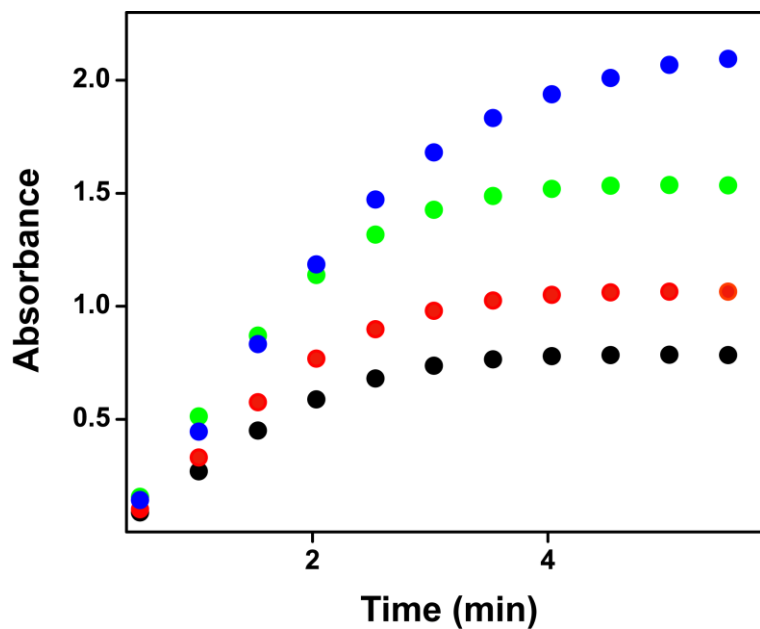


Figure S10. Formation of ClO_2 versus time. Experimental conditions: $[\text{Fe}^{\text{II}}(\text{N4Py})]^{2+} = 10 \mu\text{M}$; $[\text{ClO}_2^-] = 10.0, 8.0, 6.0, \text{ and } 4.0 \text{ mM}$ (top to bottom).

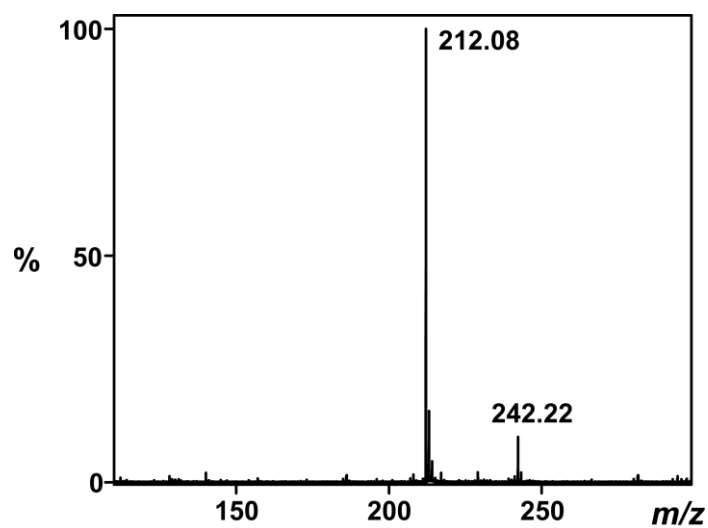


Figure S11. ESI-MS spectra of products obtained from the reaction of NaClO₂ with [Fe^{II}(N4Py)]²⁺ in presence of o-tolidine.

Part II: Computational Data.

Table S1: Absolute energies, zero-point energies and free energies of structures. All calculations are the result of a B3LYP/BS1 geometry optimization + frequency followed by B3LYP/BS2 single point calculation in the gas phase and in solvent.

Structure	E (au)	ZPE (au)	G (au)	E2 (au)	E _{solv} (au)
	BS1	BS1	BS1	BS2	BS2
¹ O ₂	-150.20746	0.00323	-150.22324	-150.30261	-150.30353
³ O ₂	-150.27026	0.00327	-150.28703	-150.36479	-150.36498
¹ H ₂ O	-76.38612	0.02054	-76.38324	-76.44381	-76.45330
¹ H ₃ O ⁺	-76.67873	0.03422	-76.66367	-76.71571	-76.83714
² H	-0.50027	0.00000	-0.51093	-0.50216	-0.50218
¹ Cl ⁻	-460.24873	0.00000	-460.26375	-460.30373	-460.41481
¹ HOCl	-535.86670	0.01004	-535.87982	-535.92431	-535.93429
¹ ClO ⁻	-535.32016	0.00125	-535.34041	-535.43276	-535.54132
² ClO	-535.25301	0.00168	-535.27327	-535.34746	-535.34998
¹ ClO ₂ ⁻	-610.39608	0.00326	-610.41877	-610.58651	-610.68895
² ClO ₂	-610.30071	0.00389	-610.32318	-610.48783	-610.49498
¹ ClO ₃ ⁻	-685.47173	0.00641	-685.49298	-685.76712	-685.86328
² ClO ₃	-685.32274	0.00515	-685.34618	-685.60688	-685.61285
¹ CH ₃ COO ⁻	-228.42964	0.04821	-228.40911	-228.59797	-228.70089
² CH ₃ COO	-228.33579	0.04759	-228.31686	-228.47898	-228.48644
¹ CH ₃ COOO ⁻	-303.51973	0.05145	-303.49712	-303.72841	-303.83767
² CH ₃ COOO	-303.46008	0.05180	-303.43806	-303.64873	-303.81785

Table S2: Absolute energies, zero-point energies and free energies of structures. All calculations are the result of a B3LYP/BS1 geometry optimization + frequency followed by B3LYP/BS2 single point calculation in the gas phase and in solvent.

Structure	E (au)	ZPE (au)	G (au)	E2 (au)	E _{solv} (au)
	BS1	BS1	BS1	BS2	BS2
¹ [Fe ^{II} (L ¹)] ²⁺	-1933.27392	0.58030	-1932.75575	-1934.22736	-1934.43607
³ [Fe ^{II} (L ¹)] ²⁺	-1933.26944	0.57940	-1932.75361	-1934.22456	-1934.43104
⁵ [Fe ^{II} (L ¹)] ²⁺	-1933.27588	0.57778	-1932.76398	-1934.23549	-1934.44662
² [Fe ^I (L ¹)] ⁺	-1933.51555	0.57694	-1933.00194	-1934.47961	-1934.54152
⁴ [Fe ^I (L ¹)] ⁺	-1933.52535	0.57412	-1933.01494	-1934.48988	-1934.55704
⁶ [Fe ^I (L ¹)] ⁺	-1933.50305	0.57289	-1932.99435	-1934.47269	-1934.54322
¹ [Fe ^{II} (L ¹)Ac] ⁺	-2162.01375	0.63208	-2161.45061	-2163.11079	-2163.17993
³ [Fe ^{II} (L ¹)Ac] ⁺	-2161.99816	0.62995	-2161.43981	-2163.09711	-2163.16530
⁵ [Fe ^{II} (L ¹)Ac] ⁺	-2161.02375	0.62879	-2161.46863	-2163.12764	-2163.19422
² [Fe ^{III} (OH)(L ¹)] ²⁺	-2009.09422	0.59531	-2008.56237	-2010.09341	-2010.29391
⁴ [Fe ^{III} (OH)(L ¹)] ²⁺	-2009.07285	0.59206	-2008.54761	-2010.07545	-2010.27598
⁶ [Fe ^{III} (OH)(L ¹)] ²⁺	-2009.08833	0.59151	-2008.56430	-2010.09680	-2010.29694
¹ [Fe ^{IV} (OH)(L ¹)] ³⁺	-2008.56786	0.59397	-2008.03705	-2009.56239	-2009.99838
³ [Fe ^{IV} (OH)(L ¹)] ³⁺	-2008.60655	0.59316	-2008.07793	-2009.60236	-2010.03838
⁵ [Fe ^{IV} (OH)(L ¹)] ³⁺	-2008.60242	0.58818	-2008.08436	-2009.60207	-2010.02709
¹ [Fe ^{II} (H ₂ O)(L ¹)] ²⁺	-2009.70520	0.60571	-2009.16405	-2010.70588	-2010.91582
³ [Fe ^{II} (H ₂ O)(L ¹)] ²⁺	-2009.68771	0.60354	-2009.15152	-2010.69068	-2010.89816
⁵ [Fe ^{II} (H ₂ O)(L ¹)] ²⁺	-2009.70745	0.60209	-2009.17489	-2010.71303	-2010.92313
² [Fe ^{III} (H ₂ O)(L ¹)] ³⁺	-2009.26192	0.60614	-2008.72102	-2010.25606	-2010.70193
⁴ [Fe ^{III} (H ₂ O)(L ¹)] ³⁺	-2009.24437	0.60369	-2008.70783		
⁶ [Fe ^{III} (H ₂ O)(L ¹)] ³⁺	-2009.24333	0.60246	-2008.70980	-2010.24870	-2010.69371
¹ [Fe ^{IV} (O)(L ¹)] ²⁺	-2008.40393	0.58437	-2007.88222	-2009.39916	-2009.59983
³ [Fe ^{IV} (O)(L ¹)] ²⁺	-2008.45211	0.58475	-2007.93075	-2009.44778	-2009.64843
⁵ [Fe ^{IV} (O)(L ¹)] ²⁺	-2008.43387	0.58223	-2007.91783	-2009.43736	-2009.63742
² [Fe ^{III} (O)(L ¹)] ⁺	-2008.72649	0.58189	-2008.20811	-2009.72677	-2009.79724
⁴ [Fe ^{III} (O)(L ¹)] ⁺	-2008.74214	0.58060	-2008.23022	-2009.75101	-2009.82006
⁶ [Fe ^{III} (O)(L ¹)] ⁺	-2008.74033	0.57995	-2008.22822	-2009.75405	-2009.82838

Table S3: Absolute energies, zero-point energies and free energies of structures. All calculations are the result of a B3LYP/BS1 geometry optimization + frequency followed by B3LYP/BS2 single point calculation in the gas phase and in solvent.

Structure	E (au)	ZPE (au)	G (au)	E _{disp} (kcal/mol)	E _{solv} (kcal/mol)
¹ [Fe ^{II} (H ₂ O)(N4Py)] ²⁺	-1362.68259	0.42939	-1362.30584	-46.20674	-142.57320
³ [Fe ^{II} (H ₂ O)(N4Py)] ²⁺	-1362.66828	0.42729	-1362.29652	-47.15309	-140.13070
⁵ [Fe ^{II} (H ₂ O)(N4Py)] ²⁺	-1362.68870	0.42611	-1362.32158	-45.05719	-140.54800
² [Fe ^{III} (OH)(N4Py)] ²⁺	-1362.06347	0.41920	-1361.69554	-45.80631	-140.81570
⁴ [Fe ^{III} (OH)(N4Py)] ²⁺	-1362.04417	0.41613	-1361.68228	-45.14647	-139.23060
⁶ [Fe ^{III} (OH)(N4Py)] ²⁺	-1362.06655	0.41532	-1361.70669	-45.42371	-137.71250
¹ [Fe ^{IV} (O)(N4Py)] ²⁺	-1361.36135	0.40786	-1361.00417	-44.90958	-141.05360
³ [Fe ^{IV} (O)(N4Py)] ²⁺	-1361.41053	0.40831	-1361.05353	-44.89556	-141.33110
⁵ [Fe ^{IV} (O)(N4Py)] ²⁺	-1361.39819	0.40643	-1361.04585	-42.92293	-140.09780
² [Fe ^{III} (O)(N4Py)] ²⁺	-1361.69233	0.40550	-1361.33835	-42.86370	
⁴ [Fe ^{III} (O)(N4Py)] ²⁺	-1361.71639	0.40430	-1361.36543	-42.66110	
⁶ [Fe ^{III} (O)(N4Py)] ²⁺	-1361.72063	0.40388	-1361.37273	-42.29000	-52.62147

Table S4: DFT calculated reaction energies and free energies (in kcal mol⁻¹) for ligand system L¹.

Reaction	Rate	Structure L ¹			
		gas-phase		solvent	
		ΔE+ZPE	ΔG	ΔE _{solv} +ZPE	ΔG _{solv}
⁵ [Fe ^{II} (H ₂ O)] ²⁺ + ClO ₂ ⁻ → ³ [Fe ^{IV} (O)] ²⁺ + H ₂ O + OCl ⁻	<i>k</i> _f	-14.82	-19.27	-18.69	-23.13
³ [Fe ^{IV} (O)] ²⁺ + ClO ₂ ⁻ → ⁴ [Fe ^{III} (O)] ⁺ + ClO ₂	<i>k</i> _{ET}	-130.57	-134.13	11.80	8.24
⁴ [Fe ^{III} (O)] ⁺ + H ₃ O ⁺ → ⁶ [Fe ^{III} (OH)] ²⁺ + H ₂ O	<i>k</i> _{PT}	-48.09	-46.41	-60.12	-58.43
³ [Fe ^{IV} (O)] ²⁺ + ClO ₂ ⁻ + H ₃ O ⁺ → ⁶ [Fe ^{III} (OH)] ²⁺ + ClO ₂ + H ₂ O	<i>k</i> _{ET+PT}	-178.66	-180.54	-48.31	-50.19
³ [Fe ^{IV} (O)] ²⁺ + ClO ₂ ⁻ + H ₂ O → ⁵ [Fe ^{II} (H ₂ O)] ²⁺ + ClO ₃ ⁻	<i>k</i> _{OAT}	-1.32	4.85	2.64	8.81
⁵ [Fe ^{II} (H ₂ O)] ²⁺ + H ₂ O + ClO ₂ → ⁶ [Fe ^{III} (OH)] ²⁺ + ClO ₂ ⁻ + H ₃ O ⁺	<i>k</i> _{CT}	155.68	156.29	31.90	32.51
⁶ [Fe ^{III} (OH)] ²⁺ + ClO ₂ ⁻ + H ₃ O ⁺ → ³ [Fe ^{IV} (O)] ²⁺ + 2 H ₂ O + ClO	<i>k</i> _r	-179.03	-184.10	-52.37	-57.44

Table S5: DFT calculated reaction energies and free energies (in kcal mol⁻¹) for ligand system N4Py.

Reaction	Rate	Structure L ¹			
		gas-phase		solvent	
		ΔE+ZPE	ΔG	ΔE _{solv} +ZPE	ΔG _{solv}
⁵ [Fe ^{II} (H ₂ O)] ²⁺ + ClO ₂ ⁻ → ³ [Fe ^{IV} (O)] ²⁺ + H ₂ O + OCl ⁻	<i>k</i> _f	-19.64	-23.12	-34.28	-37.75
³ [Fe ^{IV} (O)] ²⁺ + ClO ₂ ⁻ → ⁴ [Fe ^{III} (O)] ⁺ + ClO ₂	<i>k</i> _{ET}	-137.13	-135.73	20.01	16.76
⁴ [Fe ^{III} (O)] ⁺ + H ₃ O ⁺ → ⁶ [Fe ^{III} (OH)] ²⁺ + H ₂ O	<i>k</i> _{PT}	-34.85	-33.59	-59.19	-57.65
³ [Fe ^{IV} (O)] ²⁺ + ClO ₂ ⁻ + H ₃ O ⁺ → ⁶ [Fe ^{III} (OH)] ²⁺ + ClO ₂ + H ₂ O	<i>k</i> _{ET+PT}	-171.98	-169.32	-39.18	-40.89
³ [Fe ^{IV} (O)] ²⁺ + ClO ₂ ⁻ + H ₂ O → ⁵ [Fe ^{II} (H ₂ O)] ²⁺ + ClO ₃ ⁻	<i>k</i> _{OAT}	20.52	25.72	40.13	45.33
⁵ [Fe ^{II} (H ₂ O)] ²⁺ + H ₂ O + ClO ₂ → ⁶ [Fe ^{III} (OH)] ²⁺ + ClO ₂ ⁻ + H ₃ O ⁺	<i>k</i> _{CT}	148.36	149.89	-18.47	-16.94
⁶ [Fe ^{III} (OH)] ²⁺ + ClO ₂ ⁻ + H ₃ O ⁺ → ³ [Fe ^{IV} (O)] ²⁺ + 2 H ₂ O + ClO	<i>k</i> _r	-159.87	-147.22	-61.50	-66.75

Table S6: DFT calculated electron affinities of selected structures. All values are in kcal mol⁻¹. Experimentally reported electron affinities from the NIST Database are also given.

Reaction	EA		gas-phase		solvent	
		NIST	ΔE+ZPE	ΔG	ΔE _{solv} +ZPE	ΔG _{solv}
$\text{ClO} + \text{e}^- \rightarrow \text{ClO}^-$	-EA(ClO)	-52.52	-53.80	-53.52	-120.33	-120.06
$\text{ClO}_2 + \text{e}^- \rightarrow \text{ClO}_2^-$	-EA(ClO ₂)	-49.58	-62.32	-62.07	-122.11	-121.86
$\text{ClO}_3 + \text{e}^- \rightarrow \text{ClO}_3^-$	-EA(ClO ₃)	-98.01	-99.76	-99.18	-156.36	-155.77
$\text{CH}_3\text{COO} + \text{e}^- \rightarrow \text{CH}_3\text{COO}^-$	-EA(CH ₃ COO)		-74.28	-73.66	-134.18	-133.56
$\text{CH}_3\text{COOO} + \text{e}^- \rightarrow \text{CH}_3\text{COOO}^-$	-EA(CH ₃ COOO)		-50.22	-49.63	-12.66	-12.07
${}^3[\text{Fe}^{\text{IV}}(\text{O})(\text{L}^1)]^{2+} + \text{e}^- \rightarrow {}^4[\text{Fe}^{\text{III}}(\text{O})(\text{L}^1)]^+$			-192.89	-196.20	-110.31	-113.62
${}^5[\text{Fe}^{\text{II}}(\text{L}^1)]^{2+} + \text{e}^- \rightarrow {}^4[\text{Fe}^{\text{I}}(\text{L}^1)]^+$	-EA((L ¹)Fe ^{II})		-161.92	-160.56	-71.58	-70.22
${}^3[\text{Fe}^{\text{IV}}(\text{O})(\text{N4Py})]^{2+} + \text{e}^- \rightarrow {}^4[\text{Fe}^{\text{III}}(\text{O})(\text{N4Py})]^+$			-197.37	-200.30	-108.66	-111.59

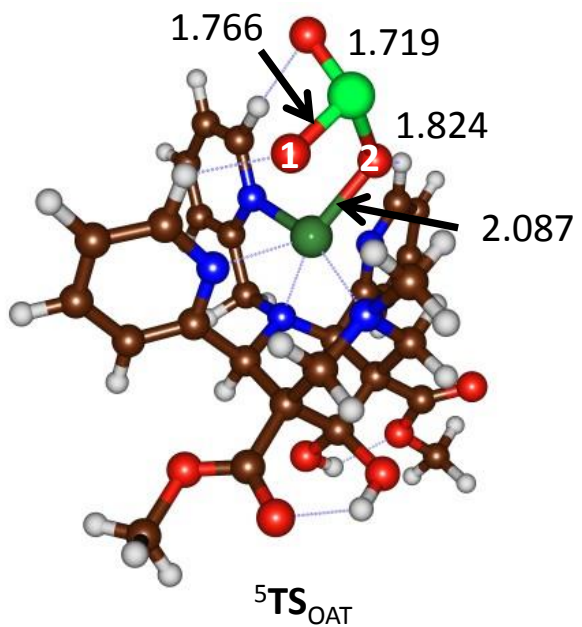


Figure S12: Optimized geometry of the oxygen addition transition state (${}^5\text{TS}_{\text{Add}}$) for the reaction of ${}^5[\text{Fe}^{\text{IV}}(\text{O})(\text{L}^1)]^{2+}$ with ClO_2^- to form $[\text{Fe}^{\text{II}}(\text{ClO}_3^-)(\text{L}^1)]^+$ products. Bond lengths are given in angstroms. The imaginary frequency displays an Fe–O₁ bond formation and simultaneous Fe–O₂ bond breaking and elongation of the O₁–Cl bond.

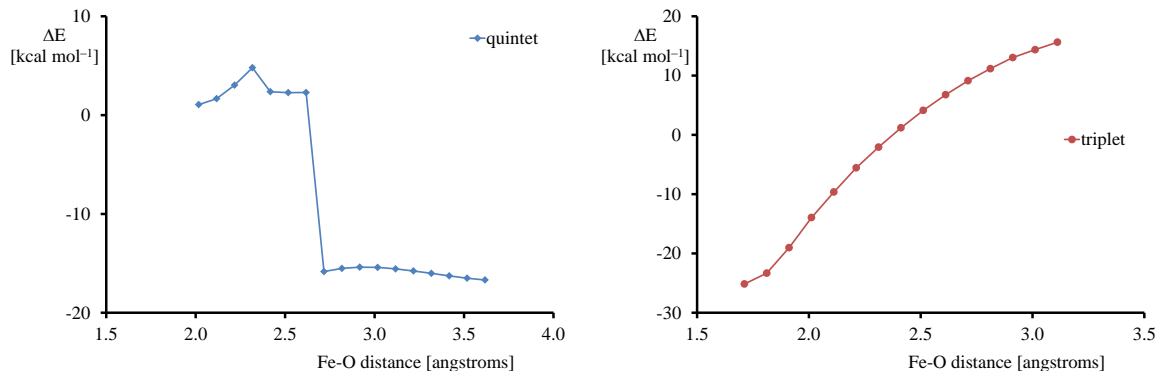


Figure S13: Geometry scans for the oxygen insertion into ClO_2^- starting from an iron(IV)-oxo species on the left-hand-side. Each data point corresponds to a full geometry optimization UB3LYP/BS1 with solvent model included and with fixed Fe–O distance. Calculations done in the quintet and triplet spin states. Energies are relative to the sum of ${}^3[\text{Fe}^{\text{IV}}(\text{O})(\text{L}^1)]^{2+}$ and ClO_2^- .

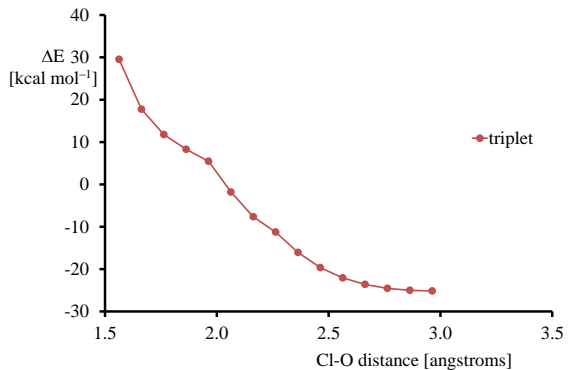


Figure S14: Geometry scan for the oxygen insertion into ClO_2^- starting from an iron(IV)-oxo species on the left-hand-side. Each data point corresponds to a full geometry optimization UB3LYP/BS1 with solvent model included and with fixed Cl–O distance. Calculations done in the quintet and triplet spin states. Energies are relative to the sum of ${}^3[\text{Fe}^{\text{IV}}(\text{O})(\text{L}^1)]^{2+}$ and ClO_2^- .

Table S7: Absolute (in au) and relative (in kcal mol^{-1}) energies of the addition transition state relative to isolated reactants. Energies obtained in Gaussian at UB3LYP/BS2 in solvent.

	E [au]	ZPE [au]	G [au]	ΔE	$\Delta E + \text{ZPE}$	ΔG
${}^5\text{TS}_{\text{OAT}}$	-2619.03535	0.58613	-2618.52115	2.05	0.87	11.80
ClO_2^-	-610.58651	0.00326	-610.60920			
${}^5[\text{Fe}^{\text{IV}}(\text{O})(\text{L}^1)]^{2+}$	-2008.45211	0.58475	-2007.93075			

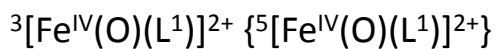
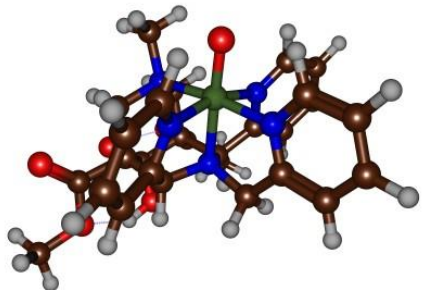
Table S8: Calculated electron transfer free energies for the reactions of ClO_2^- with either ${}^3[\text{Fe}^{\text{IV}}(\text{O})(\text{L}^1)]^{2+}$ or ${}^3[\text{Fe}^{\text{IV}}(\text{O})(\text{N4Py})]^{2+}$. All energies are in kcal mol⁻¹ and calculated using Eq 1 and 2 above. Values for r_1 and r_2 taken from the solvent calculations in Gaussian, whereby r_1 refers to ClO_2^- and r_2 the oxidant.

	${}^3[\text{Fe}^{\text{IV}}(\text{O})(\text{L}^1)]^{2+}$	${}^3[\text{Fe}^{\text{IV}}(\text{O})(\text{N4Py})]^{2+}$
r_1	3.66	3.66
r_2	7.39	5.84
λ	20.74	21.32
ΔG_{ET}	8.24 ^a	16.76 ^b
$\Delta G_{\text{ET}}^{\ddagger}$	10.10	17.04

a Data taken from Table S4.

b Data taken from Table S5.

$$r_{\text{Fe-O}} = 1.656 \{1.650\}$$
$$r_{\text{Fe-Naxial}} = 2.054 \{2.077\}$$



$$r_{\text{Fe-O1}} = 2.221 \{2.131\}$$
$$r_{\text{Fe-O2}} = 2.407 \{2.462\}$$
$$r_{\text{Fe-Naxial}} = 2.192 \{2.299\}$$
$$\text{i72} \{\text{i17}\} \text{ cm}^{-1}$$

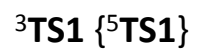
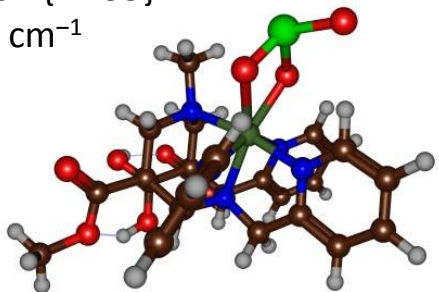


Figure S15: Optimized geometries of ${}^{3,5}[\text{Fe}^{\text{IV}}(\text{O})(\text{L}^1)]^{2+}$ as calculated with a solvent model included at UB3LYP/BS1 in Gaussian. Bond lengths are in angstroms.

1	3.192034000	0.974851000	2.126042000
6	3.021527000	0.238100000	-0.633989000
1	3.252610000	1.305973000	-0.554413000
1	3.982265000	-0.289662000	-0.626327000
6	2.474614000	-1.564473000	1.010088000
1	2.390980000	-1.600026000	2.101863000
1	3.506350000	-1.845014000	0.768457000
7	2.197043000	-0.160442000	0.555784000
8	-1.728082000	0.123623000	-0.441063000
1	-2.673814000	0.313229000	-0.539779000

⁵I(N4Py)Fe^{II}]²⁺

6	-1.950367000	-2.482521000	1.270250000
6	-2.995916000	-3.318048000	0.870019000
6	-3.604130000	-3.094170000	-0.369258000
6	-3.155317000	-2.036313000	-1.174090000
6	-2.114625000	-1.233091000	-0.711010000
7	-1.520718000	-1.457121000	0.496660000
6	-1.604770000	-0.000011000	-1.459104000
6	-2.114643000	1.233061000	-0.711010000
6	-3.155346000	2.036269000	-1.174092000
6	-3.604175000	3.094119000	-0.369261000
6	-2.995965000	3.318006000	0.870017000
6	-1.950404000	2.482494000	1.270249000
7	-1.520740000	1.457100000	0.496660000
7	-0.087758000	0.000000000	-1.418317000
6	0.560352000	1.254657000	-1.924291000
6	0.560370000	-1.254649000	-1.924290000
6	1.632778000	-1.808711000	-0.995376000
6	1.632749000	1.808738000	-0.995377000
6	2.636308000	2.648201000	-1.488057000
6	3.554757000	3.218853000	-0.600301000
6	3.454350000	2.931609000	0.766522000
6	2.442945000	2.076673000	1.197100000
7	1.547488000	1.525029000	0.335600000
7	1.547512000	-1.525004000	0.335601000
6	2.442979000	-2.076633000	1.197100000
6	3.454400000	-2.931550000	0.766521000
6	3.554811000	-3.218792000	-0.600302000
6	2.636353000	-2.648155000	-1.488057000
26	0.096839000	0.000001000	0.722984000
1	-1.445242000	-2.626147000	2.217393000
1	-3.320948000	-4.124317000	1.515788000
1	-4.413592000	-3.730738000	-0.707477000
1	-3.610182000	-1.844898000	-2.139422000
1	-3.610207000	1.844847000	-2.139424000
1	-4.413645000	3.730676000	-0.707481000
1	-3.321009000	4.124271000	1.515786000
1	-1.445283000	2.626127000	2.217393000
1	0.987161000	1.084063000	-2.919257000
1	-0.216448000	2.017787000	-2.045249000
1	-0.216418000	-2.017792000	-2.045244000
1	0.987174000	-1.084051000	-2.919257000
1	2.696859000	2.856336000	-2.550508000
1	4.336013000	3.873559000	-0.969009000
1	4.147525000	3.355889000	1.482164000
1	2.335089000	1.817352000	2.243486000
1	2.335119000	-1.817315000	2.243487000
1	4.147582000	-3.355819000	1.482163000
1	4.336079000	-3.873483000	-0.969010000
1	2.696907000	-2.856288000	-2.550508000
1	-1.985877000	-0.000015000	-2.487062000